

Flood Analysis in Peru using Satellite Image: The Summer 2017 Case

Avid Roman-Gonzalez¹, Brian A. Meneses-Claudio², Natalia I. Vargas-Cuentas³
Image Processing Research Laboratory (INTI-Lab)
Universidad de Ciencias y Humanidades
Lima, Peru

Abstract—At the beginning of the year 2017, different regions of Peru suffered from heavy rains mainly due to the 'El Niño' and 'La Niña' phenomena. As a result of these massive storms, several cities were affected by overflows and landslides. Chosica and Piura were the most affected cities. On the other hand, the satellite images have many applications, one of them is the aid for the better management of the natural disasters (post-disaster management). In this sense, the present work proposes the use of radar satellite images from Sentinel constellation to make an analysis of the most-affected areas by floods in the cities of Chosica and Piura. The applied methodology is to analyse and compare two images (one before and one after the disaster) to identify the affected areas based on differences between both images. The analysing process includes radiometric calibration, speckle filtering, terrain correction, histogram plotting, and image binarization. The results show maps of the analysed cities and identify a significant number of areas flooded according to satellite images from March 2017. Using the resulting maps, authorities can make better decisions. The satellite images used were from the Sentinel 1 satellite belonging to the European Union.

Keywords—Overflow; landslide; chosica; piura; satellite image processing; sentinel 1

I. INTRODUCTION

Our country is one of the most affected by natural phenomena due to its geo-position and the lack of the planning and prevention politics. In January, February, and March 2017, there was an intensification of rains in some districts of Peru. This escalation of rains produces the soaking of lands and the increase of the river level. This increase of the rivers level causes overflows, and the overexposure of land to the rains produces landslide called 'huaicos' in Peru. One can indicate that the intense rains have damaged urban areas in different districts as Chosica, Chaclacayo, Santa Eulalia, Cañete, Huaral, Huaura, Piura, Trujillo among others in Peru due to weak-infrastructure houses on the slopes of rivers, and on unstable ground. Several families from these communities mentioned above, they have lost their belongings, their homes, their businesses, and also human losses. One can observe in Fig. 1 some pictures of the floods in Peru.

Some consequences of nature fury, we can mention: Huaycoloro bridge collapsed due to an overflow of the river. Central highway blocked by a landslide. More than 170 houses and medical centres affected by landslides. Kilometre 66 of Cañete-Yauyos road was obstructed by landslides. Fall of street

lighting poles and power outages by landslides in Lunahuaná. Damaged crops in Quilmaná were due to flooding among others [1].

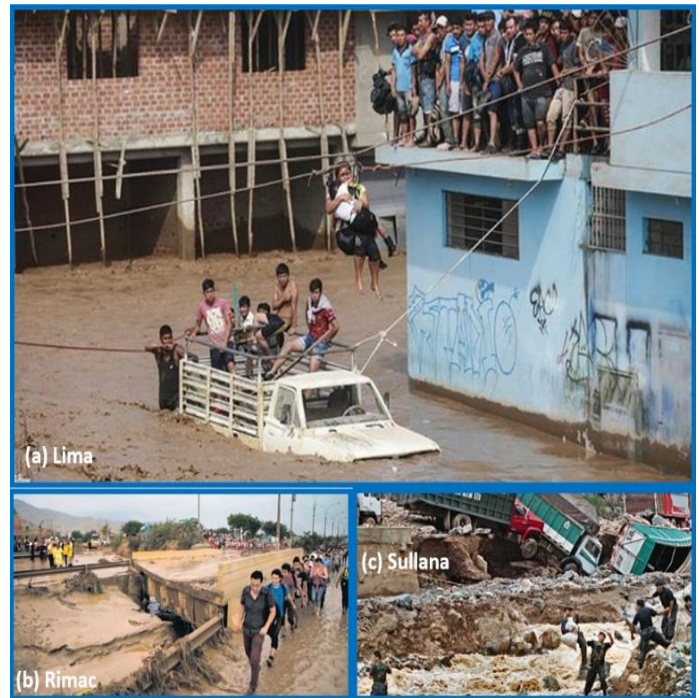
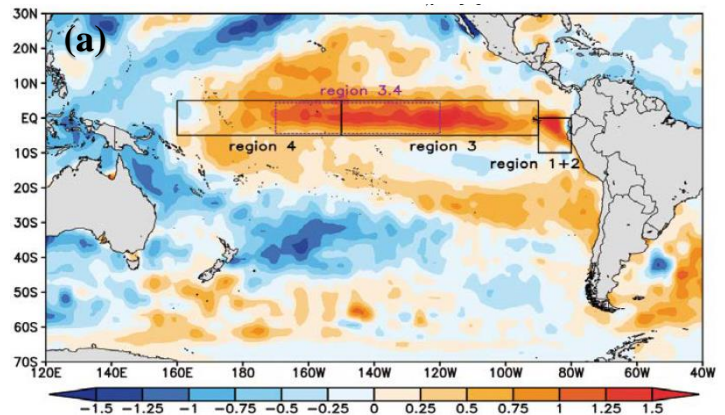
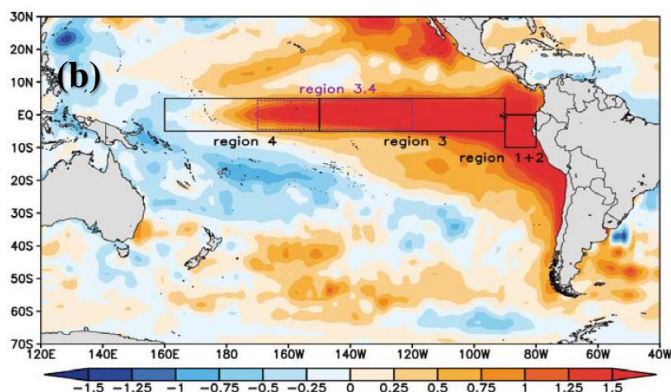


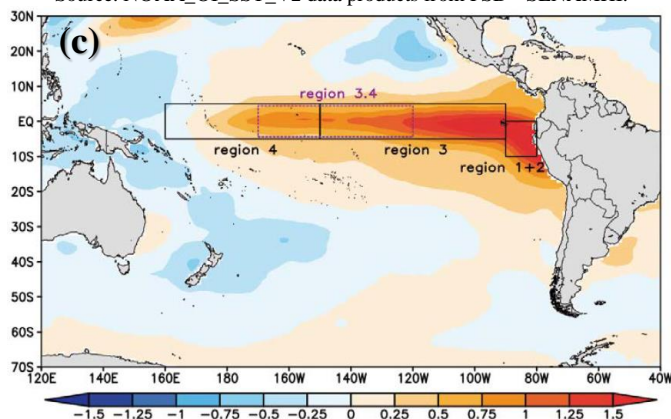
Fig 1. Image of the overflow in different cities of Peru (Lima, Rimac, and Sullana) (elcomercio.pe).



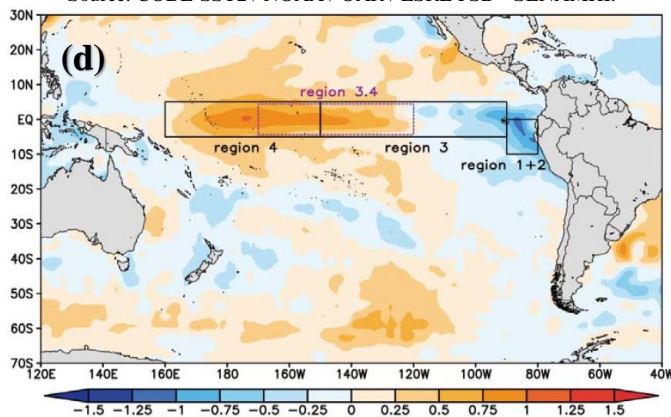
(a) Patterns of sea surface temperature anomaly (in °C) during "El Niño Extraordinario" 1982, winter period (June, July, and August). Source: NOAA_OI_SST_V2 data products from PSD - SENAMHI.



(b) Patterns of sea surface temperature anomaly (in °C) during "El Niño Extraordinario" of the year 1997, winter period (June, July, and August). Source: NOAA_OI_SST_V2 data products from PSD - SENAMHI.



(c) Patterns of sea surface temperature anomaly (in °C) during "El Niño Canónico" 1965, 1969 and 1972, winter period (June, July, and August). Source: COBE-SST2 / NOAA / OAR / ESRL PSD - SENAMHI.



(d) Patterns of sea surface temperature anomaly (in °C) during "El Niño Modoki" 1994, 2002 and 2004, winter period (June, July, and August). Source: NOAA_OI_SST_V2 data products from PSD - SENAMHI. [5].

Fig. 2. The Anomaly of Sea Surface Temperature.

After a natural disaster, one can see the structures that have considerable changes, and one concludes the seriousness of the situation. However, our vision is limited to not being able to look beyond the differences around us. In this sense, it is needed to have a broader view of the changes to get more robust conclusions about what has happened and the seriousness of the natural event.

Due to these disasters, quick decision-making is needed to define the type of support to make, and where to bring it. It is required to develop new ways of help to reduce the worsening of the emergency situation. For this purpose, the use of satellite imagery can be a great help as were already used in [2] and [3].

A satellite image shows a broader picture of the areas to be analysed. This work is a following part of the paper [4], one proposes to develop satellite image processing algorithms to analyse the areas most affected by landslides. For this purpose, we plan to use optical and radar satellite imagery because when the area under analysis is covered by clouds, optical images will not help us much, and hence the importance of having radar images whose products are not affected by the climatic conditions. Then, it is proposed to apply segmentation algorithms and identify those areas covered by water and sludge.

These floods were mainly due to the effects of the 'El Niño' and 'La Niña' phenomena. For several years, these events have been affecting our country and its consequences continue being terrible, which shows us a lack of planning and prevention. The presence of the phenomena of "El Niño" and "La Niña" over the years can be seen in Fig. 2. [5]

According to the Servicio Nacional de Meteorología de Hidrología del Perú - SENAMHI (National Meteorology Service of Hydrology of Peru), the meteorological data of precipitation of the districts of Piura and Lurigancho-Chosica from the years of 2016 - 2017 were obtained.

In Fig. 3, the pluvial rainfall plot of the district of Piura is shown. It is indicated in the months of February, March and April there is a significant increase of 222.76, 567.44 and 20.07 millimetre respectively, suggesting that in those months the strongest rains occurred in a matter of precipitation.

In Fig. 4, the rainfall plot of the Lurigancho-Chosica district is shown. It is indicated that in the months of January, February, March, October, November and December there is a notable increase of 20 mm, 18mm, 12mm, 5mm, 9mm and 11mm respectively, indicating that rains of greater intensity occurred than in the previous year.

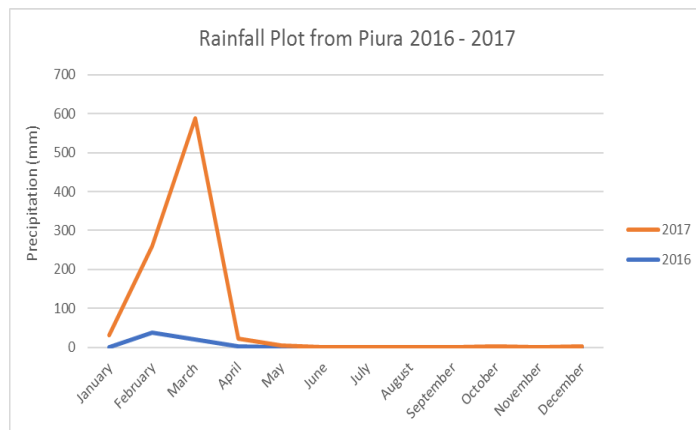


Fig. 3. Data of Precipitation of Piura District from 2016 – 2017.

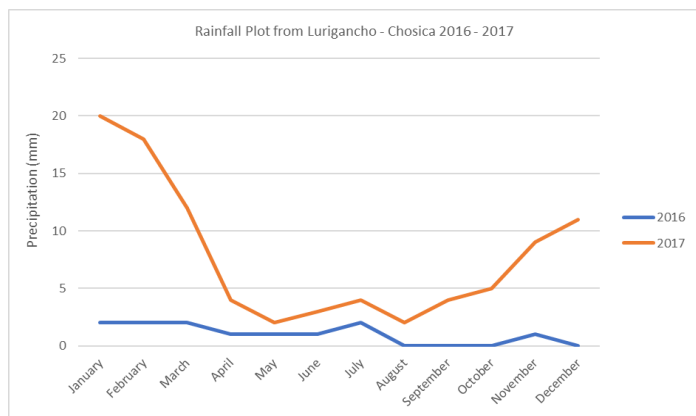


Fig 4. Data of Precipitation of Lurigiancho - Chosica district from 2016 – 2017.

The continuation of this work is organized as follows: Section 2 shows the applied methodology; in Section 3 one can see the obtained results; finally, one presents the discussion and conclusions.

II. METHODOLOGY

For the present work, it is necessary to apply some physical principles of microwave and remote sensing concepts. The methodology that we used for the analysis of overflows and floods produced by the rains is composed of three main steps:

- 1) Data Collection.
- 2) Image Processing.
- 3) Results Mapping.

A. Collection of Satellite Images

Data collection is the first step in the flow to be followed. Considering that we want to analyze territories that have been affected by overflows and floods caused by rainfall, it is very probable that these areas are covered by clouds, so the use of optical images will not give us much information. In that sense, the best option is the use of radar images. For this work, we have used radar images from the Sentinel 1A and Sentinel 1B satellites. Both satellites are part of the European constellation. To download pictures that we need, we can access the Copernicus Open Access Hub (<https://scihub.copernicus.eu>).

Sentinel-1 is a part of space mission by the European Union and carried out by the ESA (European Space Agency) within the Copernicus Program. The payload of Sentinel-1 is a Synthetic Aperture Radar (SAR) in C band. Sentinel-1A was launched on April 3rd, 2014 and Sentinel-1B on April 25th 2016 (Fig. 5).

Sentinel-1 provides continuous imagery during the day and night and regardless of weather conditions. This is particularly useful for monitoring areas prone to long periods of darkness or providing imagery for emergency response during extreme weather conditions. Sentinel-1 carries a 12 m-long advanced synthetic aperture radar (SAR), working in C-band.

Sentinel-1 has a Polar, Sun-synchronous orbit at an altitude of 693 km, it has a check time of Six days (at the equator) from the two-satellite constellation.

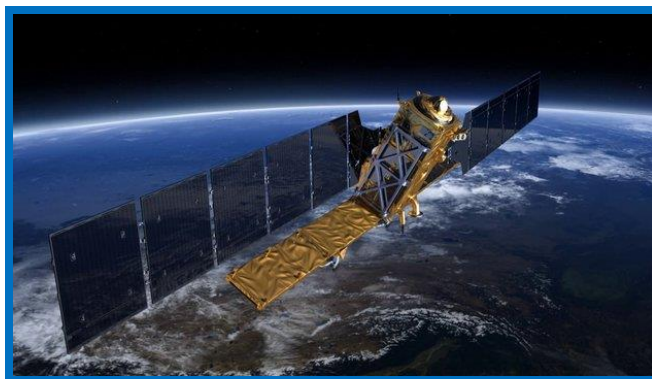


Fig 5. Sentinel-1 Source: ESA.

According to ESA website (http://www.esa.int/Our_Activities/Observing_the_Earth/Copernicus/Sentinel-1/Facts_and_figures), Sentinel-1 has different operational modes:

- Interferometric wide-swath mode at 250 km and 5×20 m resolution.
- Wave-mode images of 20×20 km and 5×5 m resolution (at 100 km intervals).
- Strip map mode at 80 km swath and 5×5 m resolution.
- Extra wide-swath mode of 400 km and 20×40 m resolution.

ESA also has a tool for Sentinel-1 application. This integrated development environment (IDE) is called SNAP (Sentinel Application Platform) and is used for science workshop [6] and [7].

The idea is to collect satellite images from date before and after disasters to compare them and analyze differences.

B. Image Processing

After data collection, the next step is to apply different image processing techniques to identify the affected areas. The pre-processing and processing techniques which were implemented in this work consists of five stages. In Fig. 6, one can observe a block diagram for this image processing step.

The signals received as raw data may contain noise from several sources like thermal noise in the receivers, quantization noise, thermal radiation from the Earth, and propagation noise [8].

The image processing step is the most critical phase of this work. The idea is to extract much information as possible from the satellite images and to achieve a useful classification of the image.

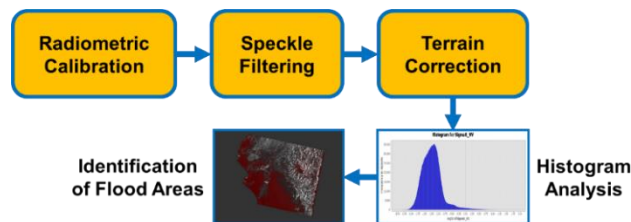


Fig 6. Image Processing Steps.

III. RESULTS

1) *Radiometric calibration*: The radiometric calibration is significant to make a quantitative interpretation rather than a qualitative interpretation. For this step, one uses the VV polarization [8], [9] and [10].

The radiometric calibration follows the equation:

$$value(i) = \frac{|DN_i|^2}{A_i^2}$$

Where depending on the selected Look Up Tables (LUT)

$$value(i) = \text{one of } \beta_i^0, \sigma_i^0 \text{ or } \gamma_i \text{ or original } DN_i$$
$$A_i = \text{one of } \text{betNought}(i), \text{sigmaNought}(i), \text{gamma}(i) \text{ or } dn(i)$$

2) *Speckle filtering*: Filtering the common speckle in the SAR image is necessary. For our cases, one uses a Gamma Map Filter and apply it to a moving window which cross the image. The size of the filter is 5 for both X and Y [11] and [12].

The speckle filtering follows the equation:

$$\hat{I}^3 - \bar{I}^2 + \sigma(\hat{I} - DN) = 0$$

where \hat{I} = sought value

\bar{I} = local mean

σ = the original image variance

DN = the input values

3) *Terrain correction*: Another essential step is to apply a geometric correction. In this work, one applies a terrain correction. For terrain correction, one uses SRTM 3sec. For DEM and image, one sets the resampling methods as bilinear interpolation. The pixel spacing in met4res should be set to 10 m. In this case, it was used “WGS84 (DD)” geographical coordinates. [13].

4) *Histogram analysis*: The flood detection methodology chosen to be used in this work relies on the unique backscattering properties of water surfaces. Water surfaces appear dark in SAR images. The retrieval methodology that was used in this work was to apply a threshold to classify an image into flooded and non-flooded portions. The threshold value can be determined manually or automatically by histogram analyzing.

5) *Identification of flooded areas*: To identify flooded areas, we apply a mask based on the threshold determined in the previous step. For better visualization, one set the mask with the red color.

C. Mapping the Results

For the results mapping, we must analyze a before-disaster, and after-disaster image, then one can show the difference between both results and identify the affected areas. For this step, we use the open source platform QGIS 2.18. [14], [15], and [16].

Our areas of analysis are Chosica and Piura. Chosica is the capital city of the Lurigancho-Chosica district of the Lima region. In Fig. 7, one can observe a map where it is possible to identify the Lurigancho-Chosica district shaded in green. Piura is the capital city of the Piura region in Peru. In Fig. 8, one can see a location map to determine the Piura district shaded with yellow border.

The datasets that we used for analyzing floods in the Chosica district were two SAR images:

- SENTINEL-1 SAR scene acquired on October 12th, 2016 in Image Mode Medium precision (IMM) with pixel size 10m. The image was acquired in vertical send-vertical received (VV) polarization configuration.
- SENTINEL-1 SAR scene obtained on March 27th, 2017 in Image Mode Medium precision (IMM) with pixel size 10m. The image was acquired in vertical send-vertical received (VV) polarization configuration.

The datasets that we used for analyzing floods in the Piura district were two SAR images:

- SENTINEL-1 SAR scene acquired on April 12th, 2016 in Image Mode Medium precision (IMM) with pixel size 10m. The image was acquired in vertical send-vertical received (VV) polarization configuration.
- SENTINEL-1 SAR scene obtained on March 20th, 2017 in Image Mode Medium precision (IMM) with pixel size 10m. The image was acquired in vertical send-vertical received (VV) polarization configuration.

After applying the methodology explained before in Section 2, we have the following results that can be seen in Fig. 9, Fig. 10, Fig. 11, Fig. 12, and Fig. 13. Fig. 9 and Fig. 10 show how was identified the threshold using the histogram analysis (separation between two crests), after choosing the limit, one creates a mask. In Fig. 11 and Fig. 12, one can observe two images that show the difference between and image before overflows and floods, and image after overflows and landslides (red areas indicates the affected areas by floods).



Fig 7. Lurigancho-Chosica district referential location. In the shaded section in dark green, it shows the location of Fig. 11 (Google Earth).

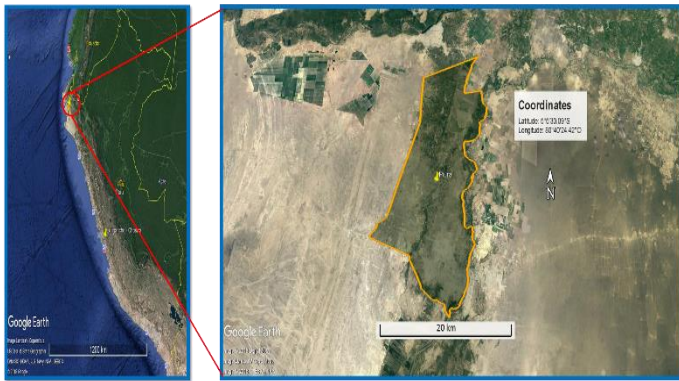


Fig 8. Piura district referential location. In the shadow with yellow border, it shows the location of Fig. 12 (Google Earth).

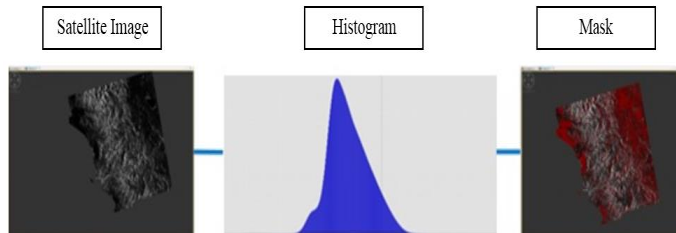


Fig 9. Referential process to use the histogram for selecting the threshold to create the mask.

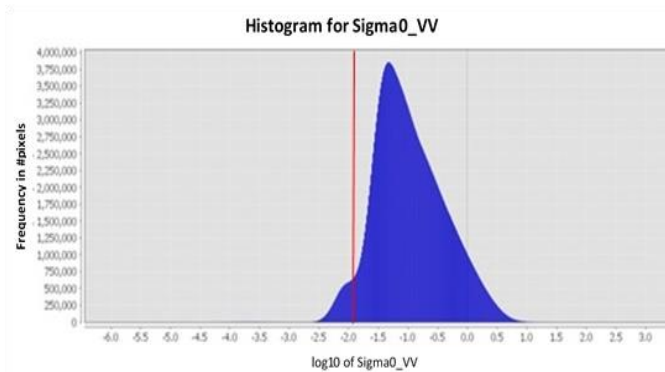
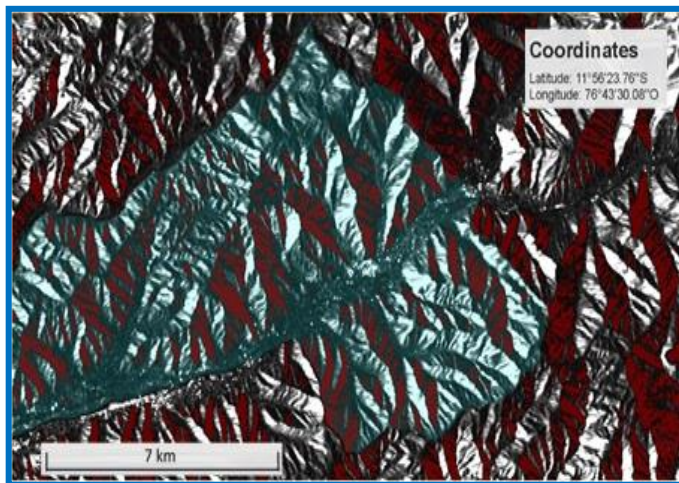
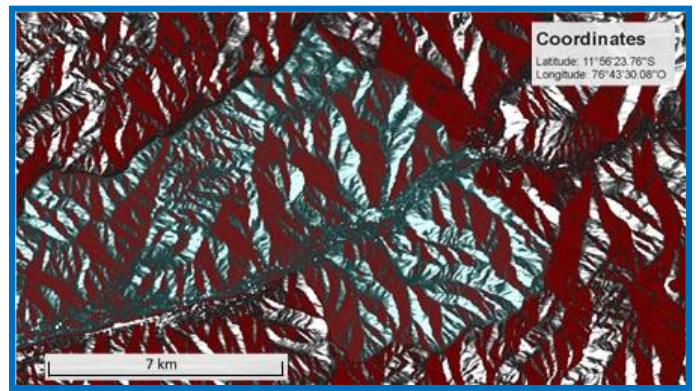


Fig 10. Selection of the threshold (red vertical line) that is the separation between the two crests.



October 2016



March 2017

Fig 11. Comparing result images for Chosica district (October 2016 and March 2017). These images were obtained after the application of the methodology described in Section 2 (especially in Fig. 6 and Fig. 9). Red areas represent the areas cover by water. One can appreciate that in March 2017 red areas are more extensive than October 2016.

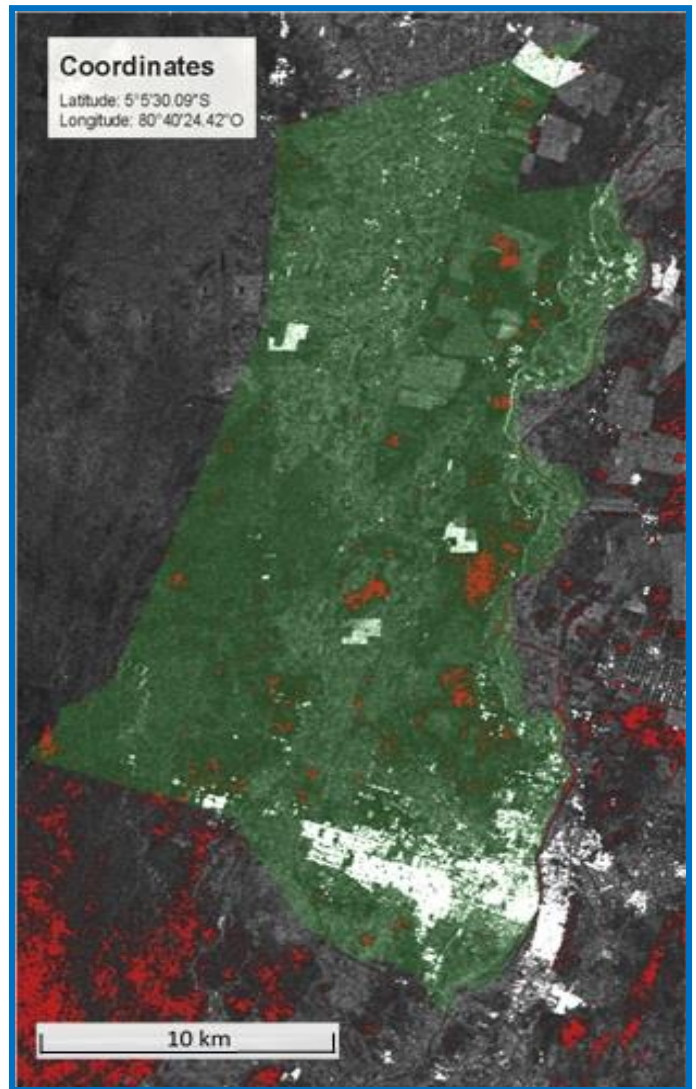


Fig 12. Comparing result image for Piura district (October 2016). This image was obtained after the application of the methodology described in Section 2 (especially in Fig. 6 and Fig. 9). Red areas represent the areas cover by water.

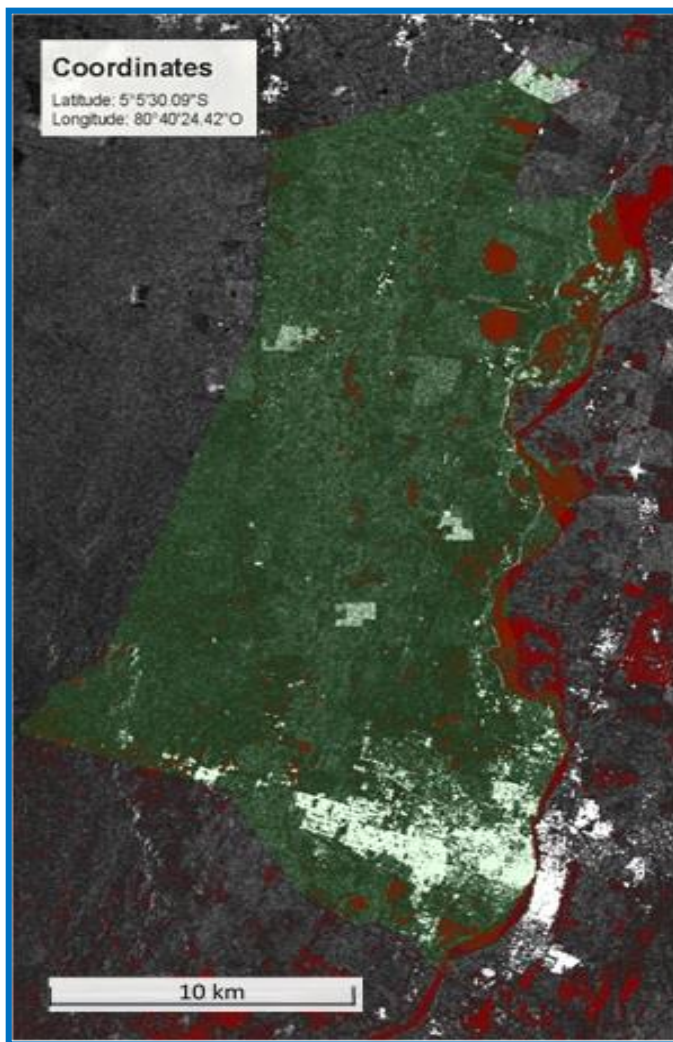


Fig 13. Comparing result image for Piura district (March 2017). This image was obtained after the application of the methodology described in Section 2 (especially in Fig. 6 and Fig. 9). Red areas represent the areas covered by water.

One can appreciate that in March 2017 red areas are more extensive than October 2016.

IV. DISCUSSION

When the optical images cannot help and the analysis area is covered by clouds, the radar images are the ones that can provide information about the affected areas.

The use of satellite images to analyze affected areas allows us to do better a post-disaster management, helping us to make better decisions: to identify the most-affected areas, to determine the contribution, to taking the type of help to manage and where to get it to the victims.

The shaded areas in red show areas affected by water, one can see a more significant covered area in the image of 2017 compared to the picture of 2016.

Talking about Piura (Fig. 12 and Fig. 13), it is possible to identify that the flow of the river (bordering the city) increased

considerably and the floods cover the principal road crossing the city and many agricultural fields.

In Fig. 12, some areas at bottom left of the October 2016 are painted in red may be due to the shadows of the mountains.

According to these results, it is necessary to save bottles of water, blankets, food, medicines to prevent a possible outbreak of dengue due to the stagnant waters.

Due to the flooded road, the help must arrive by air using helicopters as an option.

As a perspective, one hopes to continue the future work analyzing more areas in different dates.

REFERENCES

- [1] Blog de Prensa Libre Sanchez Carrion. (2018, January). ESTADO DE EMERGENCIA POR LA PRESENCIA DE HUAYCOS EN EL PERÚ.
- [2] Schwarz, B., Pestre, G., Tellman, B., Sullivan, J., Kuhn, C., Mahtta, R., ... & Hammett, L. (2018). Mapping Floods and Assessing Flood Vulnerability for Disaster Decision-Making: A Case Study Remote Sensing Application in Senegal. In *Earth Observation Open Science and Innovation* (pp. 293-300). Springer, Cham.
- [3] Wilusz, D. C., Zaitchik, B. F., Anderson, M. C., Hain, C. R., Yilmaz, M. T., & Mladenova, I. E. (2017). Monthly flooded area classification using low resolution SAR imagery in the Sudd wetland from 2007 to 2011. *Remote Sensing of Environment*, 194, 205-218.
- [4] Roman-Gonzalez, A., Vargas-Cuentas, N., & Aucapuma, L. (2017, September). Analysis of Landslide in Chosica Using Satellite Images. In *International Astronautical Congress-IAC 2017*.
- [5] SENAMHI. (2015). El Fenomeno EL NIÑO en el Peru.
- [6] Zuhlke, M., Fomferra, N., Brockmann, C., Peters, M., Veci, L., Malik, J., & Regner, P. (2015, December). SNAP (Sentinel Application Platform) and the ESA Sentinel 3 Toolbox. In *Sentinel-3 for Science Workshop* (Vol. 734, p. 21).
- [7] Twele, A., Cao, W., Plank, S., & Martinis, S. (2016). Sentinel-1-based flood mapping: a fully automated processing chain. *International Journal of Remote Sensing*, 37(13), 2990-3004.
- [8] Freeman, A., & Curlander, J. C. (1989). Radiometric correction and calibration of SAR images.
- [9] Small, D., Miranda, N., & Meier, E. (2009, July). A revised radiometric normalisation standard for SAR. In *Geoscience and Remote Sensing Symposium, 2009 IEEE International, IGARSS 2009* (Vol. 4, pp. IV-566). IEEE.
- [10] ESA. Technical Guides. Sentinel Online.
- [11] Argenti, F., Lapini, A., Bianchi, T., & Alparone, L. (2013). A tutorial on speckle reduction in synthetic aperture radar images. *IEEE Geoscience and remote sensing magazine*, 1(3), 6-35.
- [12] Nuthammachot, N., Phairuang, W., & Stratoulis, D. (2017). Removing Speckle noise in Sentinel-1A radar satellite imagery using filtering techniques. *Removing Speckle noise in Sentinel-1A radar satellite imagery using filtering techniques*.
- [13] Small, D., Miranda, N., Zuberbuhler, L., Schubert, A., & Meier, E. (2010, December). Terrain-corrected Gamma: Improved thematic land-cover retrieval for SAR with robust radiometric terrain correction. In *ESA Living Planet Symposium* (Vol. 686).
- [14] International Training Course on Space-Based Technologies for Flood and Drought Monitoring and Risk Assessment. Training Handbook, UN-SPIDER Training. 22-27 September 2016.
- [15] Roman-Gonzalez, A., & Vargas-Cuentas, N. I. (2012). Tecnología aeroespacial en el mundo. *Electro i+ d*, 1(1), 48-52.
- [16] Shah, Wahidah Md, et al. "The Implementation of an IoT-Based Flood Alert System." *INTERNATIONAL JOURNAL OF ADVANCED COMPUTER SCIENCE AND APPLICATIONS* 9.11 (2018): 620-623.